A distance constrained synaptic plasticity model of *C. elegans* neuronal network

Rahul Badhwar[1] and Ganesh Bagler[1,2,3*]
[1] *Centre for Biologically Inspired System Science, Indian Institute of Technology Jodhpur, Jodhpur, Rajasthan, India*
[2] *Dhirubhai Ambani Institute of Information and Communication Technology, Gandhinagar, Gujarat, India and*
[3] *Center for Computational Biology, Indraprastha Institute of Information Technology Delhi (IIIT-Delhi), New Delhi, India*

arXiv:1603.03867v3 [q-bio.NC] 25 Nov 2016

Brain research has been driven by enquiry for principles of brain structure organization and its control mechanisms. The neuronal wiring map of *C. elegans*, the only complete connectome available till date, presents an incredible opportunity to learn basic governing principles that drive structure and function of its neuronal architecture. Despite its apparently simple nervous system, *C. elegans* is known to possess complex functions. The nervous system forms an important underlying framework which specifies phenotypic features associated to sensation, movement, conditioning and memory. In this study, with the help of graph theoretical models, we investigated the *C. elegans* neuronal network to identify network features that are critical for its control. The 'driver neurons' are associated with important biological functions such as reproduction, signalling processes and anatomical structural development. We created 1D and 2D network models of *C. elegans* neuronal system to probe the role of features that confer controllability and small world nature. The simple 1D ring model is critically poised for the number of feed forward motifs, neuronal clustering and characteristic path-length in response to synaptic rewiring, indicating optimal rewiring. Using empirically observed distance constraint in the neuronal network as a guiding principle, we created a distance constrained synaptic plasticity model that simultaneously explains small world nature, saturation of feed forward motifs as well as observed number of driver neurons. The distance constrained model suggests optimum long distance synaptic connections as a key feature specifying control of the network.

Keywords: Brain model, *C. elegans*, feed forward motifs, synaptic plasticity, controllability, neuronal network.

I. INTRODUCTION

The quest for understanding broad structural organization, functional building blocks and mechanisms of control of nervous systems has been central to neuroscience [1]. Vast knowledge of cellular and molecular mechanisms garnered through reductionist studies over decades, while enriching our understanding of brain mechanisms, have highlighted the need for holistic perspective of neural architecture [2]. This urge to delve into systems properties has propelled efforts into connectome projects that attempt to map and model neural wirings to the finest detail possible [3–6]. *C. elegans* connectome is the only complete neuronal wiring diagram available till date [3, 7, 8]. Along with the rich understanding available on the biology of this model organism [9, 10], its connectome presents an opportunity to learn basic governing principles that drive structure and function of neuronal architecture.

Despite its apparently simple nervous system, *C. elegans* is known to possess complex functions associated to sensation, movement, conditioning and memory [11, 12]. This multi-cellular nematode has been extensively investigated to understand neural mechanisms involved in response to chemicals, temperature, mechanical stimulation as well as mating and egg laying behaviors [11, 13]. These biological functions have neuronal basis and are a reflection of emergent properties of signal dynamics over the network. Its nervous system has evolved to confer evolutionary benefits under constant tinkering and is known to undergo synaptic rewiring during the course of its life [14]. Beyond the broad evolutionary architecture, synaptic plasticity offers additional adaptive advantage to respond to the environment and perhaps to achieve better functional efficiency. The key role of distance constraint in shaping the architecture of complex networks has been well studied and highlighted [15–17].

The *C. elegans* neuronal system could be modelled as a network and studied for structural properties of its neuronal architecture as well as for network dynamics (FIG. 1). Graph theoretical studies provide important insights into evolutionary mechanisms of this system and enable biological inference. The *C. elegans* neuronal network (CeNN) has been mapped to a high resolution with details of its neurons, their locations and synaptic connectivity [18]. The network, comprising of 277 neurons that are interlinked with 2105 synapses, has been studied for its broad structural features as well as towards identification of motifs that potentially contribute to the dynamics over the network. Using graph theoretical measures, CeNN has been observed to have a small world architecture with small path length and high clustering [19]. One of the mechanisms by which interconnected systems acquire small world nature is by having modules densely connected with short-range connections, which are further interlinked through long-range connections [19]. It has been proposed that such connectivity pattern may emerge due to processes that leave the network critically poised between absolute order and extreme randomness. The small world nature may ren-

* bagler@iiitd.ac.in

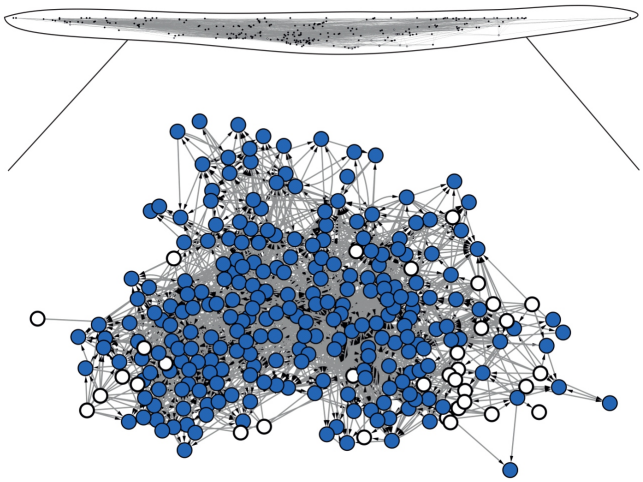

FIG. 1. Network structure of *C. elegans* nervous system. Functionally relevant driver neurons (34 nodes highlighted in white) were identified with maximum matching criterion. Beyond explaining the small world nature, saturation of feed forward motifs and observed number driver neurons, the distance constrained synaptic plasticity model accurately identifies specific driver neurons.

der this neural network (as well as other neuronal systems) efficient for information dynamics. Such a topology is known to offer evolutionary advantage by optimized wiring in neuronal systems [7, 20].

Networked systems are known to be built with recurring circuit modules that are central to their function [21]. When probing for network sub-structures that could form the building block of the CeNN, Milo *et al.* identified feed forward motifs (FFMs) to be significantly over-represented [22]. FFMs have been suggested to be of functional relevance to biological systems such as transcriptional regulatory networks [23, 24]. One of the possible utilities ascribed to these structural building blocks is control of signal regulation in response to persistent input. How exactly such building blocks may offer functional advantage to neuronal networks and whether these entities have evolved to optimize the building blocks is not clearly understood yet.

Control systems approach to complex networks provides a better perspective of dynamics over the network and ability to steer its 'state' [25]. Neuronal architecture of CeNN forms an important underlying framework which specifies phenotypic features of *C. elegans*. Important behavioral traits as well as cognitive processes (such as movement, sensation, egg laying, mechanosensation, chemosensation and memory) are known to have neuronal basis. A network is said to be controllable if it can be reached to a desired state from any initial state by providing inputs to certain nodes [25, 26]. The set of nodes that facilitate such a control are named driver nodes [25].

By studying genotypic and phenotypic aspects of CeNN, in our earlier study we have shown that 'driver neurons' are associated with important biological functions such as reproduction, signalling processes and anatomical structural development [27]. Going by their relevance to structural controllability, driver neurons are expected to be important in dictating the state of the network. In *C. elegans* driver neurons are primarily of short span and linked to motor activities [27]. Interestingly, randomized controls have no driver neurons as compared to CeNN which presents a sizeable number of driver neurons that are crucial for its control. While earlier studies have shown that connectivity of neurons in CeNN partially explains the observed number of driver neurons [25], no model has so far been developed that accounts for its small world architecture, over-representation of FFMs as well as controllability.

In this study, we create one-dimensional (1D) and two-dimensional (2D) network models of *C. elegans* neuronal system to investigate the role of FFMs as building blocks in conferring controllability and small world nature. With the help of a simple 1D ring model we show such a network is critically poised for the number of FFMs, neuronal clustering and characteristic path-length in response to synaptic rewiring, indicating optimal rewiring. We found that synaptic connections between neurons are characterized with a strong distance constraint in CeNN. Using this as a guiding principle, we created a distance constrained synaptic plasticity model that simultaneously explains small world nature, FFM saturation and controllability of the network. This model could account for the number of driver neurons observed in CeNN. Moreover, the nodes that act as driver neurons in this model match with those obtained from empirical network with high accuracy. Thus the model highlights realistic process of distance constrained synaptic plasticity as a plausible basis of nature of functional substructures and controllability observed in CeNN.

II. MATERIALS AND METHODS

A. *C. elegans* neuronal network

The nervous system of *C. elegans* consists of 277 neurons (barring the pharyngeal neurons) which are interconnected via electrical and chemical synapses [3, 18]. We constructed CeNN, a graph theoretic model of *C. elegans* neuronal network, comprising of 277 somatic neurons and 2105 synaptic connections. Multiple synaptic connections between two neurons were merged to yield a simple directed unweighted graph in which neurons represent nodes and synaptic connections are links. A typical neuron in CeNN on an average had 7.59 synaptic connections.

B. Topological properties of CeNN

We calculated following graph theoretical properties of the network embodying clustering, compactness, structural motifs and controllability of the network.

1. Clustering coefficient

Clustering coefficient of a node C_i is defined as ratio of number of triangles (triangle refers to a three node clique) made by a node with its neighbours to the maximum number of triangles that can be formed by them [19]. For a graph $G = (V, E)$ the clustering coefficient of a node i is defined as follows:

$$C_i = \frac{\mid \{e_{jk} : v_j, v_k \in N_i, e_{jk} \in E\} \mid}{k_i(k_i - 1)}$$

Here, N_i refers to the neighbourhood of node i and k_i represents its connectivity (degree).

The average clustering coefficient ($\overline{C}$) was calculated by averaging clustering coefficients of all n nodes: $\overline{C} = \frac{1}{n}\sum_{i=1}^{n} C_i$.

2. Characteristic path-length

Characteristic path-length (L) enumerates compactness, reflecting ease of information transfer, of the network. It is defined as the average of shortest path-lengths among all pairs of nodes in the network.

$$L = \frac{1}{n(n-1)} \cdot \sum_{i \neq j} d(v_i, v_j)$$

3. Feed forward motifs

Network motifs are defined as patterns of interconnections occurring in complex networks at numbers that are significantly higher than those in randomized networks [22]. In a three node digraph 13 different types of three node motifs can exist. Angular motifs are linear three node sub-structures, and triangular motifs comprise of three nodes inter-connected with either unidirectional or bidirectional edges. For our studies, we computed number of feed forward motifs, n_{FFM}, (among unidirectional triangular motifs) that are prevalent in many real world networks including CeNN [21, 22]. Please see Section S1 (FIG. S1 and FIG. S2) of Supplementary Material for more details. We used the algorithm employed by Milo *et al.* for identification and enumeration of frequency of occurrence motifs [22]. The $Zscore$, indicating significance of observed number of FFMs in CeNN, was calculated by comparing it with random controls: $Zscore = \frac{n_{FFM}(CeNN) - \overline{n_{FFM}(ER)}}{\sigma_{ER}}$.

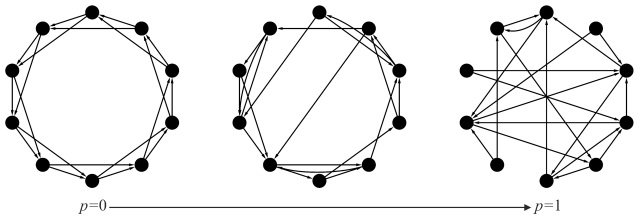

FIG. 2. The 1D ring model, with neurons linked for maximizing number of feed forward motifs, was rewired with increasing probability of synaptic rewiring. Starting with an asymptotic model (with 277 nodes and 8 out-going edges) saturated with FFMs, synaptic rewiring was emulated with probability p. The model exhibits a spectrum of topological variations between extreme regularity and randomness. The figure shows an illustration for 10 nodes and 2 outgoing edges. See FIG. S3 of Supplementary Material for another illustration.

4. Number of driver neurons

From control systems perspective, driver nodes in a network are those nodes which when controlled by an external input can provide full control over the state of the network [25]. Analogously, we term driver nodes in CeNN as driver neurons. Due to their role in control of network, driver neurons are of functional relevance to the neuronal network [27]. We computed minimum number of driver neurons (n_D) using maximum matching criterion [25]. A node is said to be matching if any matching edge is pointing towards it and is unmatched if no matching edge is directed towards it. We implemented maximum matching algorithm proposed by Pothen *et al.* to find unique unmatched nodes by augment matching [28].

C. Random controls of CeNN

We constructed two random controls of CeNN viz. Erdös-Rényi random control (ER) and degree distribution conserved control (DD) [29, 30]. In ER control, number of nodes and edges were kept the same as that of CeNN but the connectivity was random. In DD control, the in-degree and out-degree of each node was also preserved in addition to number of nodes and edges.

D. 1D ring model of CeNN

We constructed a ring graph model of CeNN so as to maximise the number of FFMs while preserving the number of neurons (n) as well as average neuronal connectivity (k) of CeNN (FIG. 2). While the core idea and strategy implemented in this model is analogous to that of Watts and Strogatz's [19], it is extended to represent directed edges (synapses), and hence naturally accommodates network motifs and controllability analysis. Starting with $n(= 277)$ nodes arranged in a circular man-

ner, every node was connected (in anti-clockwise sense) to its next nearest neighbour with a directed edge. The procedure was repeated to connect every node with its nearest neighbour and the next nearest neighbour until the out-degree of every node matched with that of average out-degree of CeNN ($k = 7.59 \approx 8$). This strategy maximises the number of FFMs to $nk(k-1)/2$ in the regular graph model of CeNN and represents an asymptotic version saturated with FFMs.

To mimic random synaptic plasticity in this simple 1D model, we rewired every edge in this network with a certain 'probability of rewiring (p)'. Every out-going edge connecting a node to its nearest neighbour was chosen and rewired randomly with probability p by ensuring that there were no duplicate edges or self-edges and that the network is always connected. In the second lap, the process was repeated for the edges made with next-nearest neighbours and so on. All edges are thus exhaustively considered for rewiring in k laps. For every probability of rewiring 1000 instances of graphs were created for a range of $p = 10^{-4}$ to $p = 1$. Topological properties ($\overline{C}$, L, n_{FFM} and n_D) were computed for every instance of graph thus generated.

E. Distance constrained models of CeNN

We created 2D distance constrained models that, similar to distance constraint observed in CeNN, follow a restraint on synaptic connectivity based on distance between two neurons. These 2D models are based on positional data of *C. elegans* neurons, that have been mapped to a high resolution [18]. In these models, the probability $P(d)$ that two neurons at a distance d are connected with a synapse approximately follows a power law pattern observed from empirical data:

$$P \propto d^{-\alpha}$$

The distance constraint is modulated by the exponent $0 \leq \alpha \leq \infty$. Here, the distance between neurons i and j, $d(i,j)$, was calculated as the Euclidean distance: $d(i,j) = \sqrt{(x_i - x_j)^2 + (y_i - y_j)^2}$. The power law nature of neuronal connectivity was established following the recipe suggested by Clauset *et al.* [31].

We created two models of CeNN based on the distance constraint: Distance constrained random (DCR) and Distance constrained synaptic plasticity (DCP).

1. Distance constrained random (DCR) model

The underlying framework for DCR model is that of ER control. Starting with ER (random) control, we rewired every edge to impose distance constraint for specific exponent α. Statistics of topological parameters were computed over 100 instances. Response of DCR model was observed by varying the value of exponent between $0 \leq \alpha \leq 3$.

2. Distance constrained synaptic plasticity (DCP) model

In contrast to DCR model, the underlying framework for DCP model is that of DD control which preserves the synaptic connectivity of each neuron. Starting with DD control, every edge was rewired to impose distance constraint for specific exponent α ($0 \leq \alpha \leq 3$) and statistics of topological parameters were computed over 100 instances.

F. Cartesian graph model of CeNN

The deterministic Cartesian graph model of CeNN was created by ensuring that every neuron is connected to its spatially nearest neurons. Beginning with ($n =$) 277 neurons placed at cartesian coordinates matching their observed position in the nervous system of *C. elegans* [18], every neuron was connected to ($k =$) 8 spatially nearest neurons. This model reflects preferential deterministic connections made by a neuron based on its distance from another neuron.

G. Identification of specific driver neurons

Using maximum matching algorithm [28], the set of specific driver nodes was identified from both the empirical neuronal network as well as its computational models (DCR and DCP). The latter were compared against the former to assess the performance of models in achieving real-like topology and control structure. The success of DCR, DCP models in accurate identification of driver neurons was measured with the help of F1 score. Using the driver neurons set identified from the CeNN (34) as the basis (Details of driver neurons is provided in Table S3 of Supplementary Material), we identified true positives (TP) and true negatives (TN) (neurons that are correctly classified) as well as false positives (FP) and false negatives (FN) (neurons that were incorrectly marked as driver neurons, and neurons that were incorrectly marked as non-driver neurons, respectively) for DCR and DCP models across 100 instances. The $F1$ score, which is used for computing the quality of binary classification is defined as, $F1 = \frac{2\ TP}{2\ TP+FP+FN}$.

III. RESULTS

A. Topological properties of CeNN

Topological features of network provide insights into its structure and function [32, 33]. Consistent with previous reports, we observed that *C. elegans* neuronal network is a small world network by virtue of high clustering coefficient ($\overline{C} = 0.172$) and comparable characteristic path length ($L = 4.018$), with respect to its randomized counterpart ($\overline{C}_{ER} = 0.028$ and $L_{ER} = 2.97$) (Table I) [19].

TABLE I. Topological properties of CeNN and its controls.

	CeNN	ER	DD
$\overline{C}$	0.172	0.028 ± 0.001	0.067 ± 0.003
L	4.018	2.97 ± 0.01	2.981 ± 0.018
n_D	34	0.28 ± 0.514	22.38 ± 1.153
n_{FFM}	3776	438.3 ± 22.1	1699.6 ± 57.5

Beyond these global topological features, CeNN is known to be over represented with feed forward motifs [22] that are functionally associated with mechanisms of memory [34]. We observed that, FFMs were significantly over-represented in CeNN ($Zscore = 151.12$) as compared to those in corresponding random graphs.

From control systems perspective CeNN can be controlled through a small set of driver neurons (34) to any desired state in finite time [25]. The number of driver neurons in CeNN is significantly higher in comparison to its random counterpart. Driver neurons in CeNN are genotypically and phenotypically associated with biological functions such as reproduction and maintenance of cellular processes [27]. This alludes to the fact that driver neurons serve a critical role in the neuronal architecture of *C. elegans* and the number of driver neurons therefore has functional bearing on its control.

Table I depicts topological features of CeNN that are potentially critical for specifying its function. Other than the small world nature, evident from high clustering among neurons, the CeNN is characterized with significantly higher number of driver nodes as well as number of feed forward motifs. While connectivity (degree) of neurons (DD) partially explains the increase in FFMs as well as that in n_D, at the same time it cannot account for observed clustering. No comprehensive model that can explain all of these functionally relevant features is hitherto known.

B. 1D ring model of CeNN

To investigate for possible mechanisms that could have lead to the observed saturation of FFMs, we created a 1D ring model of CeNN. A directed regular ring graph with n neurons and k average synapses can have a maximum of $nk(k-1)/2$ FFMs as shown in (FIG. 2). Starting from such a regular ring graph maximally saturated with 7756 FFMs, we simulated random synaptic rewiring to observe its effect on topological features. In addition to FFM saturation, the regular graph had very high average clustering coefficient ($\overline{C}_{reg} = 0.35$) as well as characteristic path-length ($L_{reg} = 17.69$). From an analogous undirected Watts and Strogatz model it was anticipated that with increase in synaptic rewiring the clustering as well as path-length would decrease to approach that of random graph asymptotically [19]. This simulation of synaptic rewiring was also expected to provide insights into its impact on number of FFMs and driver neurons.

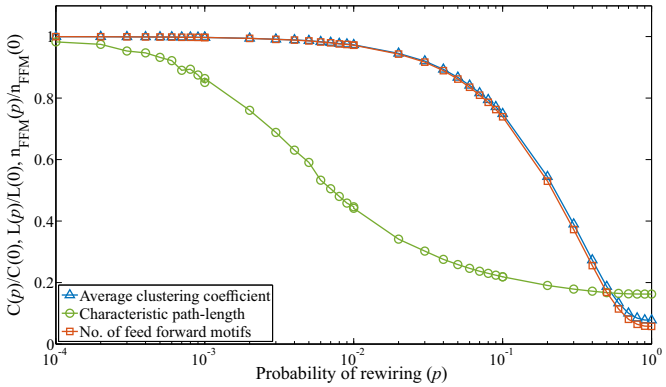

FIG. 3. Response of 1D ring model with changing probability of synaptic rewiring was measured in terms of average clustering coefficient ($\overline{C}$), characteristic path-length (L), number of FFMs (n_{FFM}) and number of driver nodes (n_D). For intermediate values of p, the model exhibits small world phenomenon as well as FFM saturation, but can not account for controllability ($n_D = 0 \ \forall \ p$). All parameters were normalized with respect to the initial ring graph ($p = 0$). Error bars represent standard deviation over 100 instances. Please see Section S3 of Supplementary Material (FIG. S4, FIG. S5 and FIG. S6) for non-normalized data.

As shown in the FIG. 3, with increasing probability of synaptic rewiring the number of FFMs is unaffected up to $p \approx 0.01$ before falling sharply. While this result points at a critical threshold for number of FFMs in response to probability of synaptic rewiring, no driver neurons were presented by the model across the simulation ($n_D \approx 0 \quad \forall \ 0 \leq p \leq 1$). For 1D ring graph, these results highlight a critical threshold of rewiring for which the network has optimum saturation of FFMs. This implies that to reflect small world nature and saturation of FFMs, the 1D representation of CeNN would need to have an optimum extent of rewiring. Such a simple model can only provide topological insights devoid of biological basis and clearly can not justify observed controllability. Search for a more realistic model prompted us to look for biological constraints that may dictate synaptic rewiring as well as to build a 2D model that could possibly reveal mechanisms that render observed controllability in CeNN.

C. CeNN follows distance constrained synaptic connectivity pattern

We measured the connectivity pattern in CeNN by enumerating number of neuron pairs that are synaptically connected and cartesian distance between them. We observed that the synaptic connections were constrained by distance as evident from the power law observed from neuronal connectivity data (FIG. 4). The probability of two neurons being connected scales as a power law ($P(d) \propto d^{-\alpha}$), with presence of a few exceptional long distance connections with an exponent $\alpha = 2.02$

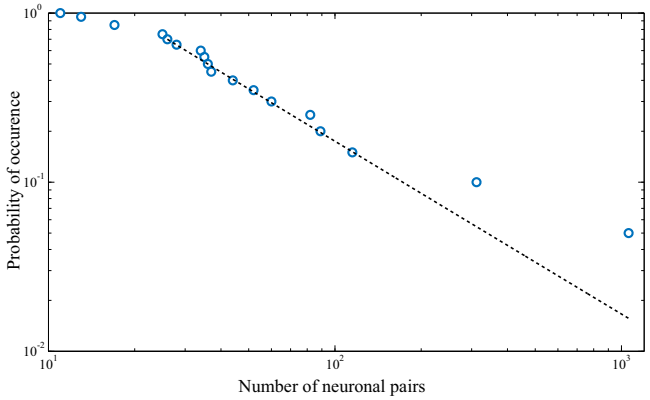

FIG. 4. Empirical distance constrained synaptic connectivity pattern observed in *C. elegans* neuronal wiring. The number of synapses that connect neurons at distance d follows a power law pattern with an exponent of $\alpha = 2.02$ (p-value=0.92) [31].

(p-value=0.92). The power law nature of data was established following the strategy prescribed by Clauset *et al.* [31].

To incorporate this empirical distance constrained connectivity pattern we created more realistic 2D models: (1) Distance constrained random (DCR) model that adds distance constraint starting from ER control, and (2) Distance constrained plasticity (DCP) model that overlays the distance constraint starting from the DD control. Along with the ER and DD random controls these models allow us to segregate the contribution of degree (connectivity) vis-à-vis distance constrained synaptic wiring towards conferring observed topological features upon CeNN.

D. Distance constrained random model

The distance constrained random (DCR) model is a 2D model in which the number of neurons, number of synapses and neuronal locations were preserved. Starting from initial random connectivity (ER) every synapse was probabilistically rewired to follow distance constraint with a certain α (FIG. 5). The lower asymptotic limit of this model converges to ER model for $\alpha = 0$. With increasing α the probability of long distance synaptic connections decreases. For extremely large values of α this model converges to the Cartesian model in which every neuron is deterministically connected to its spatially nearest neighbours. We varied the value of α between 0 and 3 to assess its impact on the topology of neural network. We found that the average clustering coefficient, characteristic path-length and number of FFMs monotonously increase with increasing α. For these parameters the DCR model was closest to actual neuronal network of *C. elegans* for $\alpha = 0.6$. While this model took us closer to CeNN, it did not reflect controllability measured in terms of n_D. The driver neurons vanish for asymptotic limits of α with maximum $n_D = 15.7$ for $\alpha = 0.4$. The fact that DD control, in which number of synapses of every neuron is preserved, matches with CeNN better in controllability (Table I) prompted us to create a more refined 'distance constrained synaptic plasticity model'.

E. Distance constrained synaptic plasticity model

The distance constrained synaptic plasticity (DCP) model preserves the number of synapses of every neuron over and above the number of neurons and their locations. While following the distance constraint, this model mimics synaptic rewiring that is known to take place in CeNN [14, 35]. We observed the response of topological features for varying extent of distance constraint ($0 \leq \alpha \leq 3$) (FIG. 5). In addition to the clustering and characteristic path-length, interestingly, this model successfully realised number of FFMs as well as number of driver neurons. We found that for an intermediate distance constraint of $\alpha = 0.6$ this model is closest to CeNN in reproducing number of driver neurons that are critical for control of the network (FIG. 5(d)). This model presents a range of distance constraint parameter ($0.6 \leq \alpha \leq 1.8$) for which the small world nature as well as functionally relevant features of regulatory motifs and controllability were realistically exhibited. The number of driver nodes in DCP model was always higher than those returned by DCR model. For $\alpha < 1.8$, i.e. in the presence of strong distance constraint, DCP model returned significantly high number of driver nodes higher than maximally displayed by DCR model. This points at the role of long distance synaptic connections in conferring observed nature of control in CeNN. This result brings out the importance of optimum heterogeneity in the range at which synapses are formed. Economizing on the synaptic lengths yields the Cartesian model ($\alpha \to \infty$), equivalent of a 2D regular graph devoid of long-range connections. In such a case control nature of DCP model is similar to that of ER model. For smaller values of α, where long range synaptic connections dominate, the model yields control response closest to reality. This highlights the important role played by long-range connections in controllability, and hence in key biological functions of the worm.

F. Identification of specific driver neurons

While the DCP model successfully reproduces key topological features important for function and control of CeNN (FIG. 5), the question is whether it can also capture specific neurons implicated in control of the network and not just the number of driver neurons (FIG. 5(d)). We compared specific neurons identified by 'the minimum driver neurons set' obtained from real-world CeNN with that obtained from distance constraint models, for

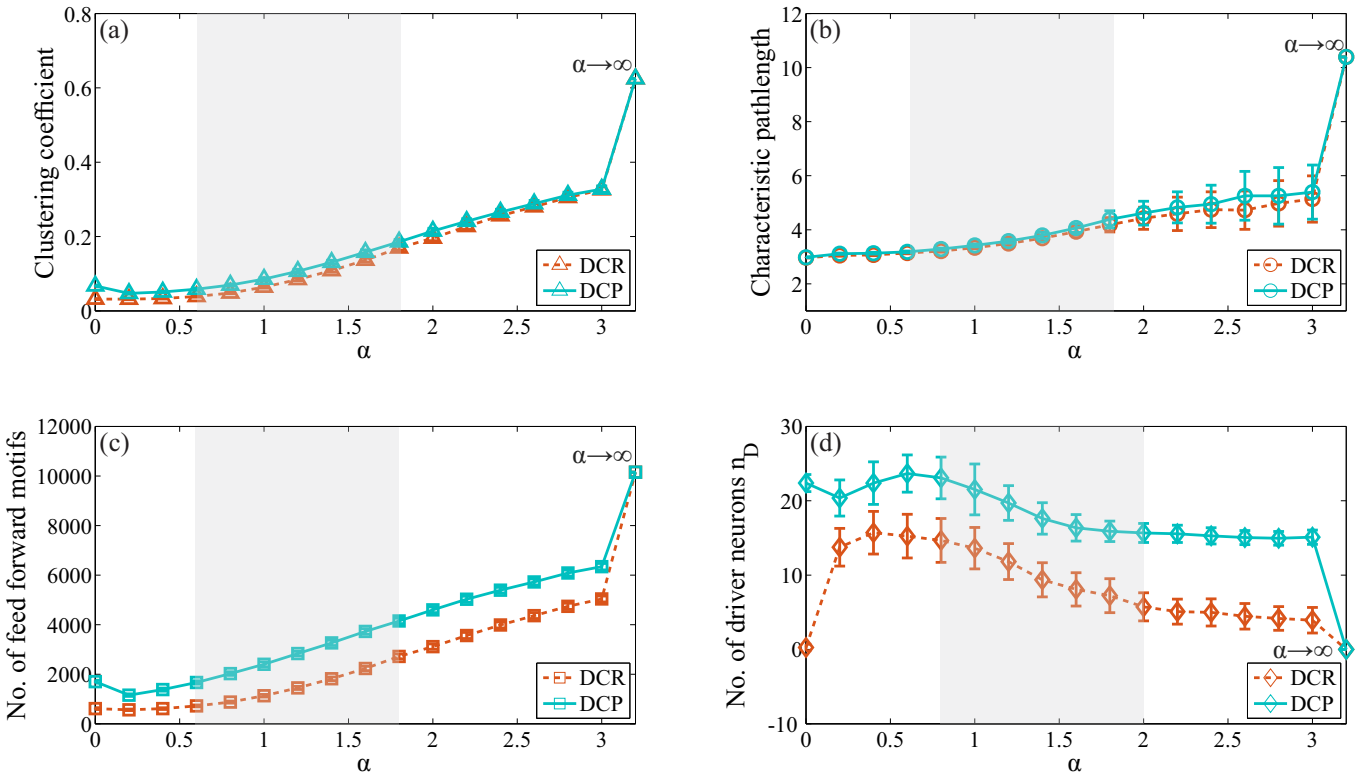

FIG. 5. Response of distance constrained models of CeNN (DCR and DCP) with increasing constraint (α) measured in terms of (a) average clustering coefficient ($\overline{C}$), (b) characteristic path-length (L), (c) number of FFMs (n_{FFM}), and (d) number of driver nodes (n_D). The lower the α more heterogeneous are the synaptic lengths (larger proportion of long range synapses). For $\alpha = 0$, DCR and DCP models converge to ER and DD controls, respectively. For asymptotic limits of $\alpha \to \infty$ both the models converge to the Cartesian model, a regular model with saturation of FFMs coupled with high clustering but devoid of driver nodes. While the small world nature (reflected in high clustering and low path-length) and FFM saturation is realized by both DCR and DCP models, DCP model stands out in reproducing all key features of CeNN for $0.6 \leq \alpha \leq 1.8$ (highlighted with gray background). Please see Figure S7, Table S1 and Table S2 of Supplementary Material for details about nature of degree distributions and associated data.

varying extent of distance constraint α (FIG. 6). Neurons that were consistently identified as driver neurons over 100 random instances of DCP and DCR models were obtained as True Positives. The classification accuracy of these models was assessed using F1 score. Interestingly, we found that the performance of DCP model was significantly better compared to DCR model (the accuracy of which was indistinguishable from that obtained from random sampling) and superior to DD control in the presence of dominant long distance connections ($\alpha \leq 1$). Thus DCP model is not only closer to real-world network in terms of number of driver nodes but also accurately identified specific neurons that can drive the network dynamics. In summary, the DCP model, that embeds empirically observed phenomenon of neuronal rewiring in addition to fixed neuronal connectivity, successfully recreates topological features of functional relevance to *C. elegans*.

IV. DISCUSSION

C. elegans connectome is one of the simplest yet complete neural diagram known to us so far. The neuronal network of this organism is responsible for many essential cognitive functions including learning and memory [12]. CeNN seemingly has evolved as a small world network with high clustering and low characteristic path-length for functional benefits [19]. Other than the small world global architecture CeNN is reported to be enriched with number of feed forward motifs among all possible three and four node motifs [22]. Our results suggest that the heterogeneous composition of motifs dictated by FFMs contributes to increased clustering as well as control of the network.

Analysis of neuronal architecture of CeNN has revealed that the network is optimally wired [7, 36] and is dictated by constraints [8, 20, 37, 38]. Till date a few simple null models of CeNN have been implemented with network feature constraints [29, 30]. These studies suggest that neuronal connectivity plays a key role in rendering clus-

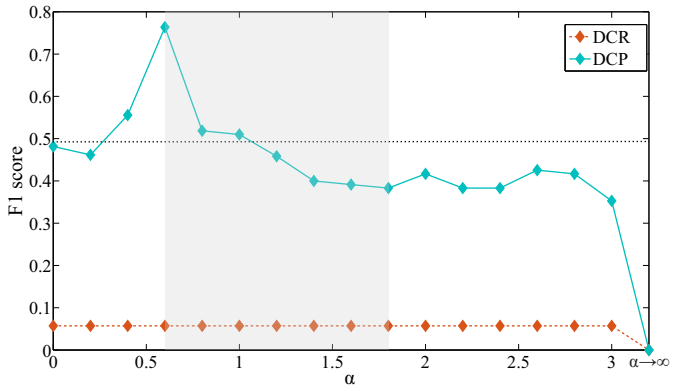

FIG. 6. Accuracy of identification of specific driver neurons with changing distance constraint exponent. The DCR model, having random synaptic connectivity pattern, fared poorly with accuracy comparable to random sampling. The performance of DCP model was consistently better than that of the DCR model indicating the critical role played by the neural connectivity and distance constraint in specifying the control of the neuronal network. For optimum distance constraint ($\alpha = 0.6$) DCP model provides the best match with the reality ($F1\ score = 0.77$), better than what could be accounted for by only neuronal connectivity (DD control; indicated with a dashed line). The spectrum of distance constraint regime for which DCP model is closest to CeNN ($0.6 \leq \alpha \leq 1.8$) is highlighted with gray background.

tering as well as presentation of as many driver neurons as observed in CeNN [25]. None of these models has been able to explain all network features, especially clustering and number of driver neurons, claimed to be of biological relevance [25, 27].

Here, we present a distance constrained synaptic plasticity model that accounts for high clustering, FFMs saturation and large number of driver nodes. With a 1D ring model maximized for feed forward motifs, we show that such a model exhibits critical phenomenon in response to increased probability of synaptic rewiring. While this simple model lends interesting insights into the mechanisms of CeNN architecture, it cannot capture the aspect of controllability. This study indicated that small-world nature, known to be important for neuronal communication, can be recreated at an optimal value of rewiring. But at the same time 1D model is incapable of exhibiting nature of control observed in the empirical network.

Rooted in empirical observation of distance constraint followed in neuronal connections, we built more realistic 2D distance constrained models with random connectivity (DCR) and degree preserved connectivity (DCP). The latter model, that mimics real-world *C. elegans* neuronal wiring and follows a distance constrained synaptic plasticity mechanism, comes closest to the CeNN in presenting small world architecture, dominance of FFMs and nature of controllability within a range of free variable α. Consistent with previous studies, number of contacts made by neurons came out as an important factor that governs network control [25, 27]. But importantly, this study brings out the key role played by long-range synaptic connections. Our results suggest that the extent of synaptic plasticity in CeNN is optimized so as to acquire key structural and dynamical network features. Thus, optimized long-range synaptic links in response to synaptic plasticity as a biologically relevant property that not only ensures small world nature, but also lends the control phenotype of this neuronal network. Further, the DCP model also successfully captures specific driver neurons with impressive accuracy. Thus beyond confirming the importance of connectivity (degree) of neurons and highlighting the role of long-range synapses as signalling conduits, this results identifies parameter value for which the model is closest to CeNN.

Structurally, the small world architecture and distance constrained connectivity mirror presence of densely connected ganglionic structures that are bridged via optimized long-range synapses [20]. From functional perspective, optimum heterogeneity in synaptic lengths is a reflection of wiring optimization in the brain architecture [7, 20, 36] of the worm that is shaped by evolution. The model reveals the role of length constrained wiring in shaping biologically important neuronal clustering [20] and saturation of functionally critical feed forward motifs [22, 23]. It also pins down specific driver neurons that have been shown to be linked with critical functions of the worm such as reproduction, signalling processes and anatomical structural development [27]. Thus, the distance-constrained plasticity model presented in this study embodies an essential structural aspect of neuronal wiring with significant biological implications for survival of the organism.

Clearly, while the DCP model highlights the role of synaptic plasticity and distance constrained neuronal connectivity in specifying structural features and control architecture of CeNN, it is limited in many ways. The present study overlooks functional differences of synaptic links such as chemical synapses and gap junctions. Also, the strength of synaptic connections (edge weight) were ignored in these unweighted network models. Models that factor in such biologically relevant aspects, which are ignored in this study in favour of simplicity, may yield more enriched representations of CeNN.

ACKNOWLEDGMENT

Ganesh Bagler acknowledges the seed grant support from Indian Institute of Technology Jodhpur (IITJ/SEED/2014/0003), and support from Dhirubhai Ambani Institute of Information and Communication Technology as well as from Indraprastha Institute of Information Technology Delhi (IIIT-Delhi). Rahul Badhwar thanks Ministry of Human Resource Development, Government of India and Indian Institute of Technology Jodhpur for the senior research fellowship.

[1] E. Kandel, J. Schwartz, and T. Jessel, *Principles of Neural Science*, 4th ed. (McGraw-Hill, 2000).
[2] O. Sporns, *Networks of the Brain* (MIT Press, 2011) p. 412.
[3] J. G. White, E. Southgate, J. N. Thomson, and S. Brenner, Philosophical Transactions of the Royal Society B: Biological Sciences **314**, 1 (1986).
[4] A.-S. Chiang, C.-Y. Lin, C.-C. Chuang, H.-M. Chang, C.-H. Hsieh, C.-W. Yeh, C.-T. Shih, J.-J. Wu, G.-T. Wang, Y.-C. Chen, C.-C. Wu, G.-Y. Chen, Y.-T. Ching, P.-C. Lee, C.-Y. Lin, H.-H. Lin, C.-C. Wu, H.-W. Hsu, Y.-A. Huang, J.-Y. Chen, H.-J. Chiang, C.-F. Lu, R.-F. Ni, C.-Y. Yeh, and J.-K. Hwang, Current Biology **21**, 1 (2011).
[5] O. Sporns, NeuroImage **80**, 53 (2013).
[6] B. Zingg, H. Hintiryan, L. Gou, M. Y. Song, M. Bay, M. S. Bienkowski, N. N. Foster, S. Yamashita, I. Bowman, A. W. Toga, and H.-W. Dong, Cell **156**, 1096 (2014).
[7] B. L. Chen, D. H. Hall, and D. B. Chklovskii, PNAS **103**, 4723 (2006).
[8] E. K. Towlson, P. E. Vértes, S. E. Ahnert, W. R. Schafer, and E. T. Bullmore, The Journal of Neuroscience **33**, 6380 (2013).
[9] Z. Altun, L. Herndon, C. Crocker, C. Wolkow, R. Lints, and D. Hall, "WormAtlas," .
[10] K. L. Howe, B. J. Bolt, S. Cain, J. Chan, W. J. Chen, P. Davis, J. Done, T. Down, S. Gao, C. Grove, T. W. Harris, R. Kishore, R. Lee, J. Lomax, Y. Li, H.-M. Muller, C. Nakamura, P. Nuin, M. Paulini, D. Raciti, G. Schindelman, E. Stanley, M. A. Tuli, K. Van Auken, D. Wang, X. Wang, G. Williams, A. Wright, K. Yook, M. Berriman, P. Kersey, T. Schedl, L. Stein, and P. W. Sternberg, Nucleic Acids Research **44**, D774 (2016).
[11] N. Chatterjee and S. Sinha, Progress in Brain Research **168**, 145 (2008).
[12] E. L. Ardiel and C. H. Rankin, Learning & Memory (Cold Spring Harbor, N.Y.) **17**, 191 (2010).
[13] O. Hobert, Journal of Neurobiology **54**, 203 (2003).
[14] E. R. Kandel, Y. Dudai, and M. R. Mayford, Cell **157**, 163 (2014).
[15] L. A. N. Amaral, A. Scala, M. Barthelemy, and H. E. Stanley, PNAS **97**, 11149 (2000).
[16] M. Barthlemy, Physics Reports **499**, 1 (2011).
[17] A. Avena-Koenigsberger, J. Goñi, R. Solé, and O. Sporns, Journal of The Royal Society Interface **12**, 20140881 (2015).
[18] W. K. Yoonsuck Choe, BH McCormick, Society of Neuroscience Abstracts **30** (2004).
[19] D. J. Watts and S. H. Strogatz, Nature **393**, 440 (1998).
[20] Y. Y. Ahn, H. Jeong, and B. J. Kim, Physica A: Statistical Mechanics and its Applications **367**, 531 (2006).
[21] U. Alon, *An Introduction to Systems Biology: Design Principles of Biological Circuits* (Chapman and Hall/CRC Press, 2007).
[22] R. Milo, S. Shen-Orr, S. Itzkovitz, N. Kashtan, D. Chklovskii, and U. Alon, Science **298**, 824 (2002).
[23] S. Mangan and U. Alon, PNAS **100**, 11980 (2003).
[24] S. Balaji, M. M. Babu, and L. Aravind, Journal of Molecular Biology **372**, 1108 (2007).
[25] Y.-Y. Liu, J.-J. Slotine, and A.-L. Barabási, Nature **473**, 167 (2011).
[26] C. Lin, Automatic Control, IEEE Transactions on **19**, 201 (1974).
[27] R. Badhwar and G. Bagler, PLoS ONE **10**, e0139204 (2015).
[28] A. Pothen and C.-J. Fan, ACM Transactions on Mathematical Software **16**, 303 (1990).
[29] P. Erdös and A. Rényi, Publicationes Mathematicae **6**, 290 (1959).
[30] S. Maslov and K. Sneppen, Science **296**, 910 (2002).
[31] A. Clauset, C. R. Shalizi, and M. E. J. Newman, SIAM Review **51**, 661 (2009).
[32] R. Albert and A. L. Barabasi, Reviews of Modern Physics **74**, 47 (2002).
[33] S. N. Dorogovtsev, *Lectures on Complex Networks* (Oxford University Press, 2010).
[34] R. Mozzachiodi and J. H. Byrne, Trends in Neurosciences **33**, 17 (2010).
[35] K. Shen and C. I. Bargmann, Cell **112**, 619 (2003).
[36] A. Pérez-Escudero and G. G. de Polavieja, PNAS **104**, 17180 (2007).
[37] R. Itzhack and Y. Louzoun, Bioinformatics **26**, 647 (2010).
[38] R. K. Pan, N. Chatterjee, and S. Sinha, PLoS ONE **5**, e9240 (2010).

SUPPLEMENTAL MATERIAL

S1. THREE NODE MOTIF CLASSIFICATION

Motifs are patterns of local connectivity among nodes that are present in numbers significantly higher than expected by chance. The pattern of connectivity among 13 three node connected digraphs could be divided into angular motifs and triangular motifs (Figure S1). Angular motifs are linear three node sub-structures, whereas triangular motifs comprise of three nodes subgraphs with either unidirectional or bidirectional edges. For our studies, we computed number of feed forward motifs, n_{FFM}, (among unidirectional triangular motifs) that are prevalent in many real world networks including CeNN. In CeNN, feed forward motifs are most prevalent among all unidirectional motifs as shown in Figure S2.

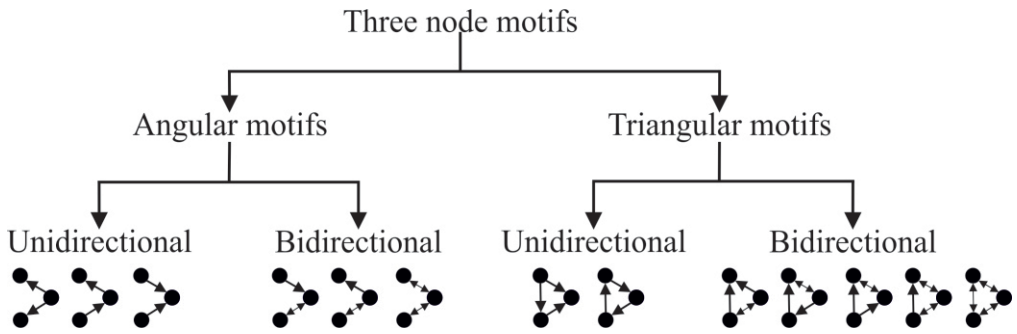

FIG. S1. Classification of three node subgraphs

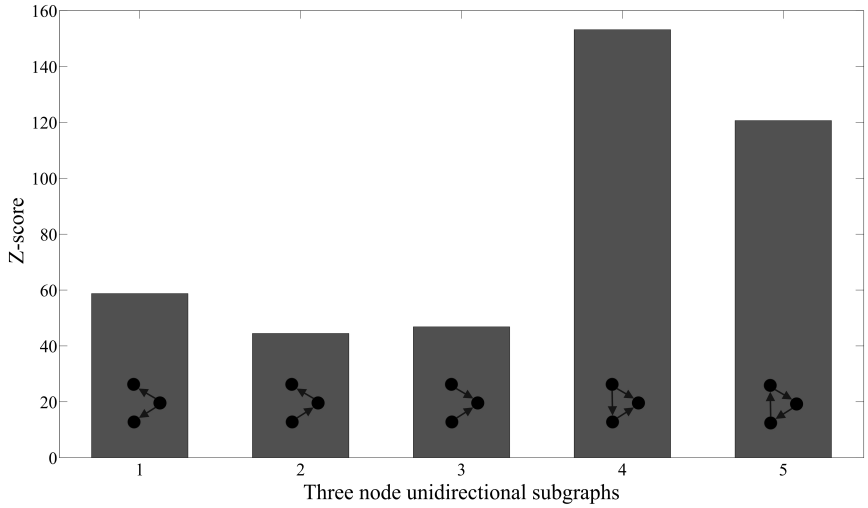

FIG. S2. Statistics for unidirectional three node motifs depicting over-representation of feed forward motifs. The Z-Score was computed in comparison to 100 instances of random controls (ER) of CeNN.

S2. 1D RING MODEL OF CENN

Following is an illustration of 1D ring model with 20 nodes and 4 outgoing synapses for every node($n = 20$ and $k = 4$) (Figure S3).

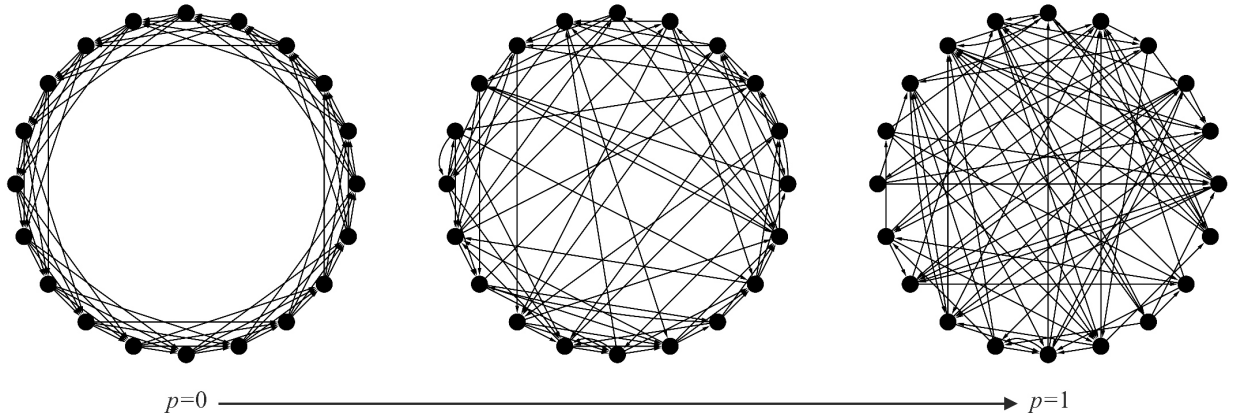

FIG. S3. Regular graph for maximum number of Feed forward motifs with graph growth. Edges are directed and point from nodes to nearest neighbours along with neighbour of neighbours and so on. This representation if for $n = 20$ and $k = 4$.

S3. RESPONSE OF CENN 1D RING MODEL TO REWIRING

Starting from a 1-D regular ring graph maximally saturated with 7756 FFMs, we simulated random synaptic rewiring to observe its effect on topological features. In addition FFMs saturation, the regular graph had very high average clustering coefficient ($\overline{C}_{reg} = 0.35$, Figure S4) as well as characteristic path-length ($L_{reg} = 17.69$; Figure S5). Figure S6 shows with increasing probability of synaptic rewiring the number of FFMs is unaffected up to $p \approx 0.01$ before falling sharply. These figures depict non-normalized data corresponding to Figure 3 in the main manuscript.

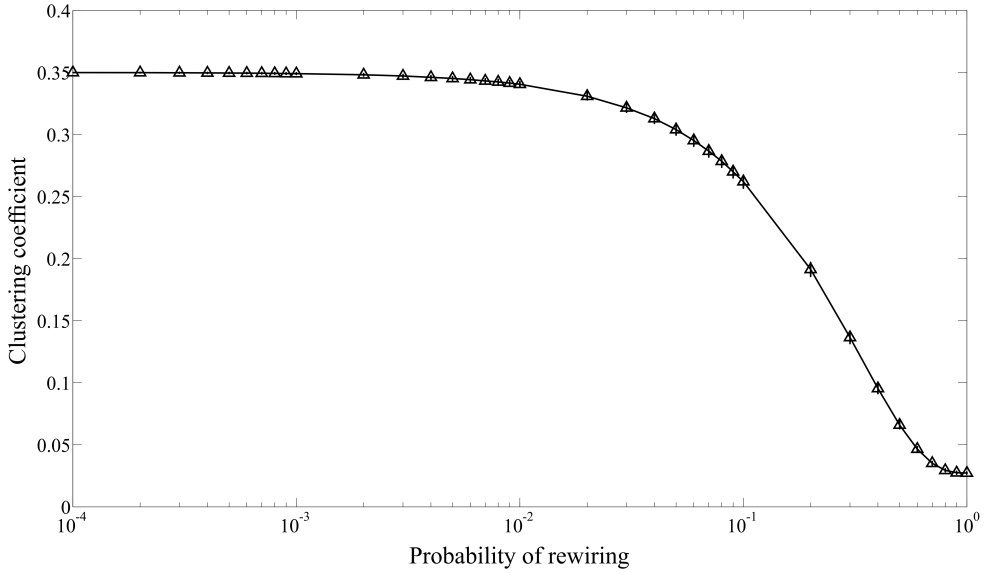

FIG. S4. Response of average clustering coefficient to rewiring.

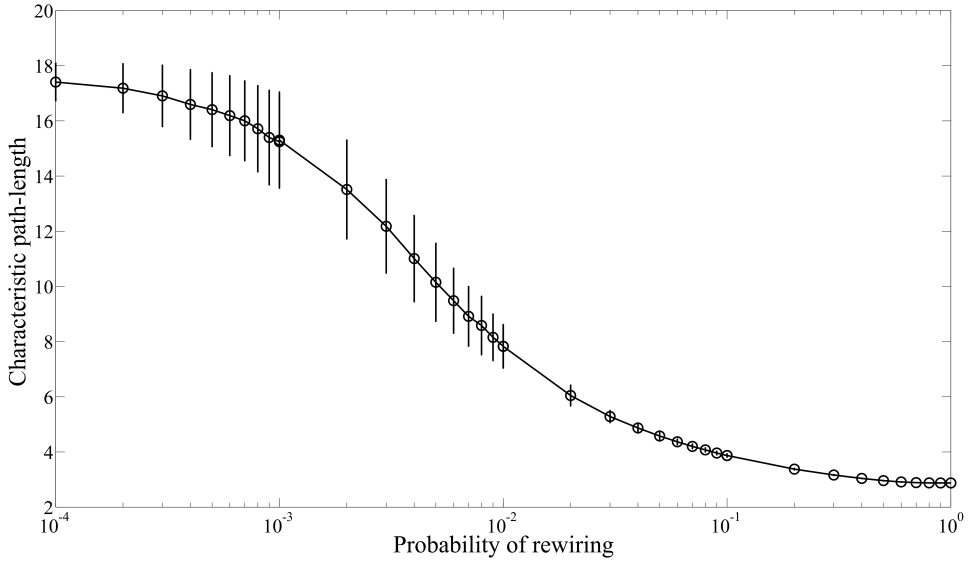

FIG. S5. Response of characteristic path-length to rewiring.

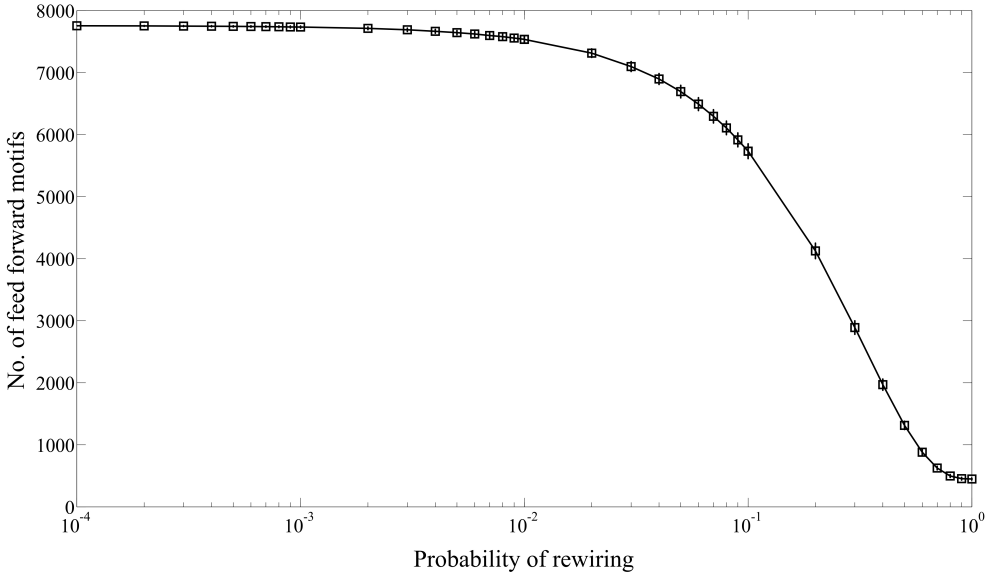

FIG. S6. Response of number of feed forward motifs to rewiring.

S4. DEGREE DISTRIBUTION OF CENN, ITS CONTROLS AND DISTANCE CONSTRAINED MODELS

Figure S7 depicts the degree distribution of CeNN in comparison to its random controls (ER and DD) as well as distance constrained models (DCR and DCP).

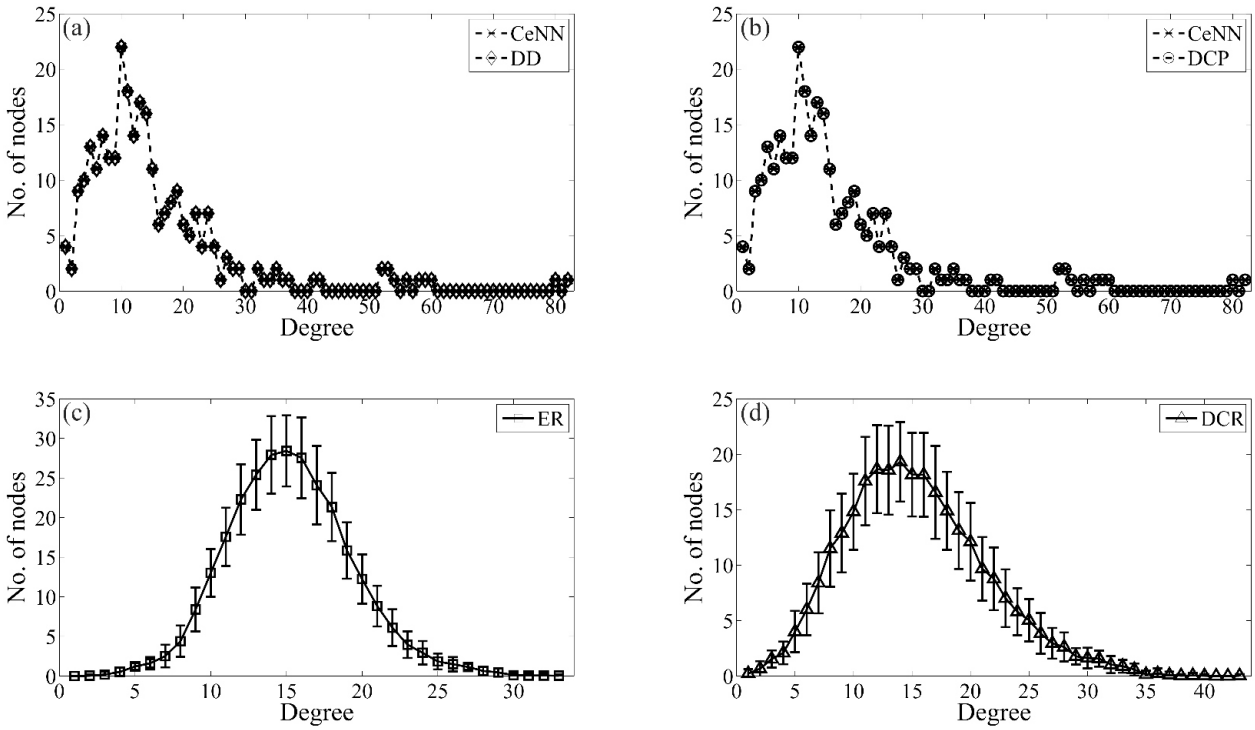

FIG. S7. Degree distributions of CeNN, its controls and distance constrained models.

S5. TOPOLOGICAL FEATURES OF DCR

TABLE S1. Differential topological properties of distance constraint random model at different values of α starting from an ER control.

Exponent	Average clustering coefficient ($\overline{C}$)	Characteristic path-length (L)	Number of driver neurons (n_D)	Number of feed forward motifs
$\alpha = 0$ (ER)	0.032 ± 0.001	2.968 ± 0.007	0.26 ± 0.441	610.55 ± 37.59
$\alpha = 0.2$	0.032 ± 0.002	3.048 ± 0.026	13.75 ± 2.536	563.91 ± 29.212
$\alpha = 0.4$	0.033 ± 0.001	3.068 ± 0.026	15.70 ± 2.866	612.19 ± 33.902
$\alpha = 0.6$	0.039 ± 0.002	3.14 ± 0.028	15.24 ± 2.934	721.21 ± 38.011
$\alpha = 0.8$	0.048 ± 0.002	3.211 ± 0.042	14.66 ± 2.952	875.83 ± 40.081
$\alpha = 1.0$	0.064 ± 0.003	3.334 ± 0.044	13.62 ± 2.784	1131.84 ± 53.844
$\alpha = 1.2$	0.085 ± 0.004	3.49 ± 0.07	11.82 ± 2.418	1447.24 ± 65.112
$\alpha = 1.4$	0.108 ± 0.004	3.689 ± 0.099	9.37 ± 2.299	1816.30 ± 73.181
$\alpha = 1.6$	0.136 ± 0.005	3.931 ± 0.14	8.08 ± 2.246	2231.32 ± 87.442
$\alpha = 1.8$	0.169 ± 0.006	4.185 ± 0.266	7.23 ± 2.287	2719.38 ± 97.224
$\alpha = 2.0$	0.196 ± 0.007	4.426 ± 0.408	5.73 ± 1.89	3114.38 ± 108.00
$\alpha = 2.2$	0.227 ± 0.008	4.589 ± 0.617	5.09 ± 1.682	3562.71 ± 121.276
$\alpha = 2.4$	0.256 ± 0.008	4.744 ± 0.661	4.98 ± 1.826	3985.73 ± 121.322
$\alpha = 2.6$	0.28 ± 0.008	4.726 ± 0.709	4.46 ± 1.72	4364.37 ± 118.252
$\alpha = 2.8$	0.305 ± 0.008	4.976 ± 0.843	4.17 ± 1.596	4738.90 ± 124.48
$\alpha = 3.0$	0.326 ± 0.008	5.138 ± 0.856	3.93 ± 1.725	5035.94 ± 120.082
$\alpha \to \infty$ Cartesian	0.624	10.394	0	10153

S6. TOPOLOGICAL FEATURES OF DCP

TABLE S2. Differential properties of distance constraint synaptic plasticity model at different values of α starting from DD control.

Exponent	Average clustering coefficient ($\overline{C}$)	Characteristic pathlength (L)	Number of driver neurons (n_D)	Number of feed forward motifs
$\alpha = 0$ (DD)	0.067 ± 0.003	2.98 ± 0.018	22.38 ± 1.153	1699.56 ± 57.496
$\alpha = 0.2$	0.047 ± 0.002	3.116 ± 0.024	20.37 ± 2.427	1155.70 ± 51.703
$\alpha = 0.4$	0.051 ± 0.002	3.133 ± 0.034	22.37 ± 2.863	1379.11 ± 61.456
$\alpha = 0.6$	0.058 ± 0.003	3.182 ± 0.033	23.66 ± 2.503	1667.59 ± 66.845
$\alpha = 0.8$	0.069 ± 0.003	3.286 ± 0.041	23.07 ± 2.808	2026.05 ± 72.395
$\alpha = 1.0$	0.086 ± 0.004	3.423 ± 0.055	21.51 ± 3.422	2402.08 ± 97.428
$\alpha = 1.2$	0.107 ± 0.005	3.58 ± 0.075	19.70 ± 2.333	2832.55 ± 89.72
$\alpha = 1.4$	0.131 ± 0.005	3.79 ± 0.112	17.62 ± 2.112	3263.43 ± 106.606
$\alpha = 1.6$	0.158 ± 0.006	4.063 ± 0.16	16.36 ± 1.784	3726.71 ± 109.069
$\alpha = 1.8$	0.186 ± 0.006	4.384 ± 0.317	15.89 ± 1.377	4150.42 ± 106.657
$\alpha = 2.0$	0.215 ± 0.007	4.615 ± 0.439	15.67 ± 1.28	4597.74 ± 114.656
$\alpha = 2.2$	0.241 ± 0.007	4.829 ± 0.576	15.55 ± 1.167	5025.00 ± 120.231
$\alpha = 2.4$	0.266 ± 0.008	4.947 ± 0.702	15.28 ± 1.092	5391.46 ± 114.416
$\alpha = 2.6$	0.288 ± 0.009	5.256 ± 0.902	15.05 ± 0.947	5722.95 ± 121.129
$\alpha = 2.8$	0.311 ± 0.008	5.256 ± 1.046	14.95 ± 0.925	6084.32 ± 118.954
$\alpha = 3.0$	0.328 ± 0.009	5.395 ± 1.002	15.10 ± 0.959	6339.36 ± 131.354
$\alpha \to \infty$ Cartesian	0.624	10.394	0	10153

S7. LIST OF *C. ELEGANS* NEURONS

Table S3 lists all 277 neurons with their X- and Y-coordiantes. Rows depicting the 34 driver neurons identified in this study are shown in grey.

TABLE S3. Driver neurons of CeNN.

Neuron Name	**X**	**Y**
ADAL	0.01106776858176	0.00590280993408
ADAR	0.01420641977856	0.00220444444224
ADEL	0.01623272728896	0.00565685948544
ADER	0.01494123459264	0.00930765433152
ADFL	0.08239338844992	-0.00098380167552
ADFR	0.0832790123616	-0.00318419750784
ADLL	0.08263933883904	-0.01303537187328
ADLR	0.0832790123616	-0.01151209877376
AFDL	0.08632859503296	-0.0027054545184
AFDR	0.08646320986944	-0.0009797530656
AIAL	0.06517685948544	0.00934611567936
AIAR	0.05903012343744	0.01151209877376
AIBR	0.07544098765824	0.00612345676416
AIML	0.0332033058048	0.01795438019136
AIMR	0.0374755555776	0.01518617284416
AINL	0.06197950412928	-0.0061487603232
AINR	0.06196938269376	-0.00342913581888
AIYR	0.0394350617088	0.01518617284416
AIZL	0.04869818180736	0.0027054545184
AIZR	0.05756049380928	0.00318419750784
ALA	0.09405629632128	-0.01322666665344
ALML	-0.37848615384768	-0.01678769230464
ALMR	-0.3815384615232	-0.00610461541056
ALNL	-0.9800451284544	-0.04944102563136
ALNR	-0.9862451280576	-0.04944102563136
AQR	0.01959506172864	0.00416395063296
AS1	-0.0164108642208	0.0247387654272
AS10	-0.8348061541056	0.03357538460928
AS11	-0.8440584613248	0.02330564102208
AS2	-0.10988307691392	0.03968000001984
AS3	-0.19839999998016	0.03968000001984
AS4	-0.28386461537088	0.03968000001984
AS5	-0.40137846156288	0.04273230769536
AS6	-0.47616	0.04273230769536
AS7	-0.57536000001984	0.04273230769536
AS8	-0.6654030769536	0.03968000001984
AS9	-0.7584984613248	0.0351015384768
ASEL	0.069112066128	0.00049190083776
ASER	0.07176691358784	-0.00073481481408
ASGL	0.0779662809696	-0.00762446283648
ASGR	0.08009481479424	-0.01028740739712
ASHL	0.07550677684032	0.00049190083776
ASHR	0.07838024691456	-0.0009797530656
ASIL	0.0769824793536	-0.01278942148416
ASIR	0.07715555553792	-0.01175703702528
ASJL	0.06345520658304	0.00664066116096
ASJR	0.06270419750784	0.00906271602048
ASKL	0.08854214877312	-0.01008396696576
ASKR	0.08866765431168	-0.00955259258304

Neuron Name	X	Y
AUAL	0.06862016529024	0.0061487603232
AUAR	0.06711308639232	0.00538864195008
AVAL	0.08952595038912	0.0017216529024
AVAR	0.09087209875392	-0.00024493825152
AVBL	0.069112066128	-0.0044271074208
AVBR	0.07176691358784	-0.0063683950752
AVDL	0.06173355374016	-0.00147570245376
AVDR	0.06637827157824	-0.00146962962816
AVEL	0.08288528922816	0.00221355374016
AVER	0.08401382717568	0.00318419750784
AVFL	0.01861530866304	0.02277925923648
AVFR	0.02449382717568	0.02253432098496
AVG	0.00195950619072	0.02449382717568
AVHL	0.07206347109504	-0.00860826445248
AVHR	0.07642074072384	-0.0127367901504
AVJL	0.06763636361472	-0.00934611567936
AVJR	0.07299160496448	-0.00979753083456
AVKL	0.02680859503296	0.01770842974272
AVKR	0.03184197531648	0.01592098765824
AVL	0.06098962962816	0.00906271602048
AVM	-0.34796307691392	0.0228923077152
AWAL	0.0779662809696	-0.00295140496704
AWAR	0.07838024691456	-0.00538864195008
AWBL	0.07919603303424	-0.00393520658304
AWBR	0.08278913579904	-0.00685827157824
AWCL	0.07845818180736	0.00491900825856
AWCR	0.07862518516608	0.00416395063296
BAGL	0.1128912396768	0.00049190083776
BAGR	0.11463111111552	0.00318419750784
BDUL	-0.13277538462912	-0.00152615386752
BDUR	-0.13430153843712	0.00457846154304
CEPDL	0.09419900825856	-0.01623272728896
CEPDR	0.09601580245248	-0.01249185183936
CEPVL	0.10748033058048	0.0113137190304
CEPVR	0.10507851853248	0.01494123459264
DA1	-0.02302419754752	0.02424888886464
DA2	-0.12819692308608	0.03815384615232
DA3	-0.23350153845696	0.04120615382784
DA4	-0.37390769230464	0.04120615382784
DA5	-0.52652307691392	0.03968000001984
DA6	-0.6989784613248	0.03815384615232
DA7	-0.8409107693376	0.03204923074176
DA8	-0.9039917949888	0.0038789743488
DA9	-0.9077117949888	0.00263897436864
DB1	-0.01224691358784	0.02522864198976
DB2	0.01175703702528	0.02424888886464
DB3	-0.12056615386752	0.03815384615232
DB4	-0.2731815384768	0.03968000001984

Neuron Name	X	Y
DB5	-0.46852923078144	0.04120615382784
DB6	-0.657772307616	0.03815384615232
DB7	-0.827175384768	0.03204923074176
DD1	-0.00808296295488	0.0247387654272
DD2	-0.18924307689408	0.03815384615232
DD3	-0.37848615384768	0.04120615382784
DD4	-0.5829907692384	0.04120615382784
DD5	-0.767655384768	0.0366276922848
DD6	-0.895311794592	0.00511897438848
DVA	-0.9444984613248	-0.03786769232448
DVB	-0.939951794592	-0.03580102561152
DVC	-0.951525128256	-0.03786769232448
FLPL	0.02336528922816	0.00910016529024
FLPR	0.02498370367872	0.00391901232192
HSNL	-0.53873230767552	0.00915692308608
HSNR	-0.54178461541056	0.0351015384768
IL1DL	0.12814016529024	-0.01451107438656
IL1DR	0.12687802470336	-0.0100424691456
IL1L	0.12641851238784	-0.00098380167552
IL1R	0.12418370369856	0.00244938269376
IL1VL	0.12912396696576	0.01180561980864
IL1VR	0.11218172842176	0.01322666665344
IL2DL	0.13674842974272	-0.0157408264512
IL2DR	0.137410370352	-0.01396148146752
IL2L	0.13158347109504	-0.00295140496704
IL2R	0.13030716052224	-0.00073481481408
IL2VL	0.13404297522432	0.01303537187328
IL2VR	0.12687802470336	0.01224691358784
LUAL	-0.9730184615232	-0.02050769230464
LUAR	-0.9833517947904	-0.0180276922848
OLLL	0.128632066128	-0.0061487603232
OLLR	0.1290824691456	-0.00440888888448
OLQDL	0.12272925619392	-0.01598677684032
OLQDR	0.1217343210048	-0.01224691358784
OLQVL	0.11608859503296	0.00418115703168
OLQVR	0.114386172864	0.00759308639232
PDA	-0.9300317949888	-0.00025435895808
PDB	-0.9130851284544	0.00305230767552
PDEL	-0.6821907691392	-0.0122092307616
PDER	-0.6928738460928	0.02136615384768
PHAL	-0.958551794592	-0.01596102563136
PHAR	-0.9606184617216	-0.01678769230464
PHBL	-0.980871794592	-0.01513435895808
PHBR	-0.9767384615232	-0.0180276922848
PHCL	-1.0172451284544	-0.01637435899776
PHCR	-1.0139384615232	-0.02381435899776
PLML	-1.0250984615232	-0.0184410256512
PLMR	-1.0230317949888	-0.01720102561152

Neuron Name	X	Y
PLNL	-1.0085651280576	-0.0143076922848
PLNR	-0.970125128256	-0.01761435897792
PQR	-0.9903784617216	-0.0143076922848
PVCL	-0.9767384615232	-0.0403476922848
PVCR	-0.9899651280576	-0.03042769232448
PVDL	-0.6959261537088	-0.0122092307616
PVDR	-0.6989784613248	0.01831384617216
PVM	-0.7035569230464	-0.00915692308608
PVNL	-1.0242717947904	-0.03249435897792
PVNR	-1.018071794592	-0.0333210256512
PVPL	-0.895725128256	0.00966564100224
PVPR	-0.8783651280576	0.01338564100224
PVQL	-0.9630984613248	-0.01926769232448
PVQR	-0.9531784617216	-0.02422769230464
PVR	-0.9945117947904	-0.03869435899776
PVT	-0.8824984617216	0.0150389743488
PVWL	-0.9990584615232	-0.0180276922848
PVWR	-1.0077384613248	-0.03621435897792
RIAL	0.08952595038912	-0.00393520658304
RIAR	0.08989234568832	-0.004653827136
RIBL	0.07034181819264	0.0044271074208
RIBR	0.07103209877376	0.00514370369856
RICL	0.05583074380608	0.0061487603232
RICR	0.05290666667328	0.00489876544704
RID	0.09871012345728	-0.0164108642208
RIFL	0.00440888888448	0.02449382717568
RIFR	0.01665580247232	0.02302419754752
RIGL	-0.0063683950752	0.0247387654272
RIGR	0.0083279012064	0.02302419754752
RIH	0.07993388432064	0.009592066128
RIML	0.06443900825856	0.00245950412928
RIMR	0.0668681481408	0.00342913581888
RIPL	0.12149950412928	-0.00664066116096
RIPR	0.12099950619072	-0.00318419750784
RIR	0.0695624691456	0.00930765433152
RIS	0.03453629632128	0.01616592590976
RIVL	0.07304727271104	-0.01820033058048
RIVR	0.07617580247232	-0.01690074072384
RMDDL	0.07895008264512	0.00934611567936
RMDDR	0.07715555553792	0.01224691358784
RMDL	0.08731239670848	0.0051649587072
RMDR	0.0879328394976	0.00514370369856
RMDVL	0.09419900825856	-0.00295140496704
RMDVR	0.09724049382912	-0.00195950619072
RMED	0.1155966941952	-0.01795438019136
RMEL	0.11264528922816	-0.00295140496704
RMER	0.11291654323584	-0.00024493825152
RMEV	0.09405629632128	0.0173906172864

Neuron Name	X	Y
RMFL	0.069112066128	0.01278942148416
RMFR	0.07127703702528	0.01224691358784
RMGL	0.00885421490112	0.0034433058048
RMGR	0.00955259258304	0.00171456787968
RMHL	0.07304727271104	0.00910016529024
RMHR	0.0722567901504	0.0100424691456
SAADL	0.07772033058048	0.00934611567936
SAADR	0.07838024691456	0.01151209877376
SAAVL	0.0944449587072	-0.00590280993408
SAAVR	0.09454617282432	-0.0026943210048
SABD	-0.0026943210048	0.02424888886464
SABVL	0.0247387654272	0.02228938273344
SABVR	0.02032987654272	0.02277925923648
SDQL	-0.6898215384768	-0.01068307689408
SDQR	-0.14651076925824	-0.00305230767552
SIADL	0.06837421490112	0.01082181819264
SIADR	0.06147950619072	0.01494123459264
SIAVL	0.05189553716352	0.0140191735488
SIAVR	0.05462123455296	0.01126716052224
SIBDL	0.079687933872	0.00688661155008
SIBDR	0.07984987654272	0.0073481481408
SIBVL	0.07427702477568	0.01008396696576
SIBVR	0.073236543216	0.00979753083456
SMBDL	0.0646849587072	0.0140191735488
SMBDR	0.05731555555776	0.01690074072384
SMBVL	0.05952	0.01426512393792
SMBVR	0.06613333332672	0.0127367901504
SMDDL	0.07255537187328	0.01328132232192
SMDDR	0.07078716052224	0.0146962962816
SMDVR	0.09381135801024	-0.00489876544704
URADL	0.1313375206464	-0.01205157025728
URADR	0.12491851851264	-0.0083279012064
URAVL	0.11658049587072	0.00934611567936
URAVR	0.11340641973888	0.01126716052224
URBL	0.12100760329152	-0.00295140496704
URBR	0.12222419750784	-0.00122469137664
URXL	0.09223140496704	-0.01180561980864
URXR	0.09307654319616	-0.0100424691456
URYDL	0.12568066116096	-0.01205157025728
URYDR	0.13055209877376	-0.00955259258304
URYVL	0.12149950412928	0.00221355374016
URYVR	0.12099950619072	0.00710320988928
VA1	-0.0026943210048	0.0247387654272
VA10	-0.8088615384768	0.03357538460928
VA11	-0.7857784617216	0.02785230769536
VA12	-0.8911784615232	0.00842564102208
VA2	-0.07020307689408	0.0366276922848
VA3	-0.14498461539072	0.03815384615232
VA4	-0.23960615386752	0.03968000001984

Neuron Name	**X**	**Y**
VA5	-0.34338461537088	0.04273230769536
VA6	-0.44563692306624	0.04273230769536
VA7	-0.54636307689408	0.04273230769536
VA8	-0.6257230767552	0.03968000001984
VA9	-0.71424	0.0366276922848
VB1	0.01494123459264	0.02400395061312
VB10	-0.7386584615232	0.0366276922848
VB11	-0.8180184613248	0.03357538460928
VB2	0.0293925925632	0.02351407405056
VB3	-0.08088615384768	0.0366276922848
VB4	-0.16024615382784	0.03815384615232
VB5	-0.25181538462912	0.04120615382784
VB6	-0.3693292307616	0.04273230769536
VB7	-0.45632000001984	0.04273230769536
VB8	-0.56315076925824	0.04120615382784
VB9	-0.6364061537088	0.04120615382784
VC1	-0.1663507692384	0.03815384615232
VC2	-0.2609723077152	0.04120615382784
VC3	-0.39680000001984	0.04273230769536
VC4	-0.49752615384768	0.03815384615232
VC5	-0.53262769232448	0.04273230769536
VC6	-0.6531938458944	0.04120615382784
VD1	-0.02179950617088	0.02424888886464
VD10	-0.77376	0.0366276922848
VD11	-0.8485415386752	0.03357538460928
VD12	-0.8684451284544	0.01751897436864
VD13	-0.9147384613248	0.0001589743488
VD2	-0.03086222225088	0.02424888886464
VD3	-0.13430153843712	0.03815384615232
VD4	-0.21976615382784	0.04120615382784
VD5	-0.31438769230464	0.04273230769536
VD6	-0.40595692310592	0.04425846156288
VD7	-0.4883692307616	0.04120615382784
VD8	-0.5967261541056	0.04273230769536
VD9	-0.6882953843712	0.03815384615232